Networks and Heterogeneous Media

https://www.aimspress.com/journal/nhm

NHM, 21(1): 183–197.
DOI: 10.3934/nhm.2026008
Received: 24 November 2025
Revised: 15 January 2026
Accepted: 22 January 2026
Published: 27 January 2026

Research article

Bifurcation and pattern dynamic behavior in a fractional-order ecosystem model

Hai Yan Zhang[1], **Wei Zhang**[2,*] **and Hao Lu Zhang**[3,*]

[1] School of Physics and Electronic Information Engineering, Jining Normal University, Ulanqab, Inner Mongolia 012000, China

[2] Institute of Economics and Management, Jining Normal University, Ulanqab, Inner Mongolia 012000, China

[3] College of Civil Engineering, Inner Mongolia University of Technology, Hohhot 010051, China

* **Correspondence:** Email: jnsfxyzw@163.com, 18586053173@163.com.

Abstract: This paper investigates the dynamic behavior of a fractional-order reaction-diffusion system for vegetation pattern formation, incorporating interactions between plant biomass, soil water, and salt concentration. The model utilizes Grünwald–Letnikov fractional derivatives to capture memory effects and anomalous diffusion. A novel high-order numerical scheme is developed, featuring a high-accuracy, short-memory time discretization with a nine-point finite difference method in space to enhance stability. Bifurcation analysis is performed to determine equilibrium stability and identify Turing instability thresholds. Numerical simulations illustrate the emergence of diverse vegetation patterns, highlighting how different fractional orders influence spatiotemporal dynamics. Overall, the proposed framework provides an effective computational tool for analyzing complex fractional ecological systems.

Keywords: high-precision numerical method; stability analysis; bifurcation analysis

1. Introduction

Vegetation patterns in semi-arid regions have long been a subject of intensive research due to their ecological significance and mathematical complexity. These patterns provide valuable critical insights into ecosystem resilience and the processes that may lead to desertification [1, 2]. Early modeling efforts primarily attributed pattern formation to water scarcity and infiltration-feedback mechanisms [3, 4]. However, recent more studies have shown that vegetation patterns can also emerge in water-sufficient environments, indicating that additional mechanisms–such as plant-soil feedbacks (PSFs) play a crucial roles [5, 6].

The role of autotoxicity—where plants modify soil properties through litter decomposition, subsequently inhibiting their own growth—has been recognized as a significant driver of vegetation dynamics [6, 7]. Abbas et al. [5] compared several reaction-diffusion models incorporating autotoxicity, and highlighted how different growth terms and additional factors influence biomass distribution. Iuorio and Veerman [7] further demonstrated that autotoxicity can induce movement and deformation of vegetation spots, a phenomenon not observed in classical biomass-water models.

Fractional-order derivatives have recently been introduced into ecological modeling to capture memory effects and anomalous diffusion processes that integer-order models may overlook [8–10]. Gao et al. [8] investigated pattern dynamics in a fractional vegetation-water model, while Zhang et al. [10] and Yang et al. [11] extended this approach to plankton dynamics and chemical oscillations, respectively. These studies demonstrate the rich dynamical behaviors that fractional calculus can introduce into ecological systems.

Competition between plant species and their coexistence mechanisms represent another important aspect of vegetation dynamics. Eigentler and Sherratt [12] showed that metastable states can facilitate species coexistence through long transients, while Gai and Kolokolnikov [13] analyzed resource-mediated competition between species with different water intake rates. These studies reveal how subtle differences in species traits can determine community structure.

From a mathematical perspective, the analysis of reaction-diffusion systems has benefited from various analytical and numerical approaches. Broadbridge and colleagues [14–16] developed conditionally integrable models based on non-classical symmetries, with applications to soil-water-plant dynamics. Numerical methods have also advanced significantly, with Li et al. [17, 18] and Wang et al. [19] developed reproducing kernel techniques, while other studies employed spectral methods [20, 21] and high-order discretization schemes [22, 23].

In this work, we investigate a three-component fractional reaction-diffusion system describing the interactions between plant biomass, soil water, and salt concentration. The model extends previous approaches by incorporating fractional time derivatives for all components, enabling us to examine how distinct memory effects influence pattern formation. We conduct a comprehensive bifurcation analysis to identify stability conditions and Turing instability thresholds, and we develop a high-order numerical scheme combining Grünwald-Letnikov discretization in time with a nine-point finite difference scheme in space. Our work builds on the foundations laid by Xue [24–26] in fractional calculus and extends existing vegetation modeling frameworks to include salinity dynamics, thereby providing new insights into the complex interplay among multiple resources in arid ecosystems.

We consider the following reaction-diffusion system describing the dynamics of plant biomass (B), soil water (W), and salt concentration (S):

$$\begin{cases} \mathcal{D}_t^{\alpha_1} B = \Lambda W B(1-B) - MB + D_B \nabla^2 B, \\ \mathcal{D}_t^{\alpha_2} W = P - N(1-RB)W - \Gamma \dfrac{W^2}{W^2+1} B + D_W \nabla^2 W, \\ \mathcal{D}_t^{\alpha_3} S = Q - KS + D_S \nabla^2 S, \end{cases} \tag{1.1}$$

where the description of variables and parameters is shown in Table 1.

The main contributions of this paper are:

- Developed a three-component fractional-order reaction-diffusion model incorporating plant biomass, soil water, and salt concentration dynamics using Grünwald–Letnikov derivatives,

extending classical vegetation models to capture memory effects and anomalous diffusion processes.

- Established a novel high-order numerical scheme combining p-order generating functions for temporal discretization with a nine-point finite difference method for spatial discretization, achieving $O(\tau^p)$ accuracy with recursive coefficient computation for enhanced stability.
- Performed a comprehensive bifurcation analysis to identify stability conditions and Turing instability thresholds across different fractional orders, with numerical simulations demonstrate how memory effects significantly influence vegetation pattern formation and ecosystem dynamics.

Table 1. Description of variables and parameters.

Symbol	Description
B	Vegetation biomass
W	Soil water content
S	Soil salinity concentration
∇^2	Laplace operator in two dimensions: $\frac{\partial^2}{\partial x^2} + \frac{\partial^2}{\partial y^2}$
Λ	Plant growth rate influenced by water availability
M	Natural mortality rate of vegetation
P	Precipitation rate
N	Evaporation rate coefficient
R	Reduction of evaporation due to vegetation cover
Γ	Maximum water uptake rate by vegetation
Q	Salt input rate
K	Natural salt removal (decay) rate
t, x, y	Time variable and spatial variables
$\alpha_1, \alpha_2, \alpha_3$	Orders of fractional derivatives for B, W, and S, respectively
$\mathcal{D}_t^{\alpha_i}$	Grünwald–Letnikov fractional derivative operator of order α_i
D_B, D_W, D_S	Diffusion coefficients for vegetation, water, and salt

This paper is organized as follows. Section 2, presents the bifurcation and stability analysis of the fractional-order system. Section 3, we develop a high-order numerical scheme combining Grünwald-Letnikov discretization in time with a nine-point finite difference method in space. Section 4, reports numerical simulations of the pattern dynamical behavior. Finally, Section 5, concludes the paper.

2. Bifurcation analysis

The equilibrium states of the system are obtained by setting the time derivatives to zero:

$$\begin{cases} \Lambda WB(1-B) - MB = 0, \\ P - N(1-RB)W - \Gamma \dfrac{W^2}{W^2+1} B = 0, \\ Q - KS = 0, \end{cases} \tag{2.1}$$

which yields two biologically meaningful equilibria:

$$E_0 = \left(0, \frac{P}{N}, \frac{Q}{K}\right), \quad E_1 = \left(B^*, \frac{M}{\Lambda(1-B^*)}, \frac{Q}{K}\right), \tag{2.2}$$

where B^* is determined by the implicit equation

$$P - N(1-RB^*)\frac{M}{\Lambda(1-B^*)} - \Gamma\frac{\left(\frac{M}{\Lambda(1-B^*)}\right)^2}{\left(\frac{M}{\Lambda(1-B^*)}\right)^2+1}B^* = 0. \tag{2.3}$$

Here E_0 represents the desert state (no vegetation), while E_1 corresponds to a vegetated state.

The linearization of the system around any state (B, W, S) is given by

$$J(B,W,S) = \begin{bmatrix} \Lambda W(1-2B) - M - D_B k^2 & \Lambda B(1-B) & 0 \\ NRW - \Gamma\dfrac{W^2}{W^2+1} & -N(1-RB) - \dfrac{2\Gamma BW}{(W^2+1)^2} - D_W k^2 & 0 \\ 0 & 0 & -K - D_S k^2 \end{bmatrix}, \tag{2.4}$$

where k denotes the spatial wave number.

At the desert equilibrium E_0, this reduces to

$$J(E_0) = \begin{bmatrix} \Lambda\dfrac{P}{N} - M - D_B k^2 & 0 & 0 \\ RP - \Gamma\dfrac{(P/N)^2}{(P/N)^2+1} & -N - D_W k^2 & 0 \\ 0 & 0 & -K - D_S k^2 \end{bmatrix}. \tag{2.5}$$

To analyze stability in the fractional-order framework, we define Let $n = \mathrm{lcm}(\mathrm{denom}(\alpha_1), \mathrm{denom}(\alpha_2), \mathrm{denom}(\alpha_3))$, where $\mathrm{denom}(\alpha)$ denotes the denominator of the rational number α in its reduced form. The characteristic equation is:

$$\begin{vmatrix} \Lambda\dfrac{P}{N} - M - D_B k^2 - \lambda^{n\alpha_1} & 0 & 0 \\ RP - \Gamma\dfrac{(P/N)^2}{(P/N)^2+1} & -N - D_W k^2 - \lambda^{n\alpha_2} & 0 \\ 0 & 0 & -K - D_S k^2 - \lambda^{n\alpha_3} \end{vmatrix} = 0.$$

The eigenvalues are given by

$$\lambda^{n\alpha_1} = \frac{\Lambda P}{N} - M - D_B k^2, \qquad \lambda^{n\alpha_2} = -N - D_W k^2, \qquad \lambda^{n\alpha_3} = -K - D_S k^2.$$

According to the fractional-order stability criterion [27], if all eigenvalues λ_i satisfy $|\arg(\lambda_i)| > \dfrac{\pi}{2n}$, then the system at the equilibrium point is globally asymptotically stable. If there exists at least one eigenvalue λ_i satisfying $|\arg(\lambda_i)| < \dfrac{\pi}{2n}$, then the system at the equilibrium point is unstable. If

$\max_i\{|\arg(\lambda_i)|\} = \dfrac{\pi}{2n}$, then the system undergoes a bifurcation. The corresponding wave number satisfying this condition is called the critical wave number.

Turing bifurcation occurs at

$$\max(|\arg(\lambda_1)|, |\arg(\lambda_2)|, |\arg(\lambda_3)|) = \frac{\pi}{2n}. \tag{2.6}$$

When $\dfrac{\Lambda P}{N} - M < 0$, the system without diffusion (i.e., $D_B = D_W = D_S = 0$) at E_0 is globally asymptotically stable.

The instability condition requires that there exists at least one eigenvalue λ_i satisfying

$$|\arg(\lambda_i)| < \frac{\pi}{2n}. \tag{2.7}$$

Specifically, when $\dfrac{\Lambda P}{N} - M - D_B k^2 > 0$, we have

$$|\arg(\lambda_1)| = 0 < \frac{\pi}{2n}, \tag{2.8}$$

which indicates that the system at E_0 is unstable in this case.

At E_1, the Jacobian matrix is

$$J(E_1) = \begin{bmatrix} a_{11} - D_B k^2 & a_{12} & 0 \\ a_{21} & a_{22} - D_W k^2 & 0 \\ 0 & 0 & a_{33} - D_S k^2 \end{bmatrix}, \tag{2.9}$$

where

$$a_{11} = -\frac{MB^*}{1-B^*}, \quad a_{12} = \Lambda B^*(1-B^*), \quad a_{21} = NRW^* - \Gamma\frac{(W^*)^2}{(W^*)^2+1},$$
$$a_{22} = -N(1-RB^*) - \frac{2\Gamma B^* W^*}{((W^*)^2+1)^2}, \quad a_{33} = -K,$$

with $W^* = \dfrac{M}{\Lambda(1-B^*)}$.

For the fractional-order system, using the transformation $\mu = \lambda^{1/n}$, where $n = \mathrm{lcm}(\mathrm{denom}(\alpha_1), \mathrm{denom}(\alpha_2), \mathrm{denom}(\alpha_3))$, the characteristic equation becomes:

$$\det\left(\mathrm{diag}(\mu^{n\alpha_1}, \mu^{n\alpha_2}, \mu^{n\alpha_3}) - J(E_1)\right) = 0. \tag{2.10}$$

So,

$$(\mu^{n\alpha_3} - a_{33} + D_S k^2) \cdot \left[(\mu^{n\alpha_1} - a_{11} + D_B k^2)(\mu^{n\alpha_2} - a_{22} + D_W k^2) - a_{12}a_{21}\right] = 0. \tag{2.11}$$

The first factor gives

$$\mu^{n\alpha_3} = a_{33} - D_S k^2 = -K - D_S k^2. \tag{2.12}$$

The second factor corresponds to the plant-water interactions. Letting $p = a_{11} - D_B k^2$, $q = a_{22} - D_W k^2$, $r = a_{12}$, $s = a_{21}$, we have

$$(\mu^{n\alpha_1} - p)(\mu^{n\alpha_2} - q) - rs = 0. \tag{2.13}$$

Expanding Eq (2.13), we can get

$$\mu^{n(\alpha_1+\alpha_2)} - q\mu^{n\alpha_1} - p\mu^{n\alpha_2} + (pq - rs) = 0. \tag{2.14}$$

According to the stability criterion for the system, we can get the following conclusion.

The system is asymptotically stable if and only if $|\arg(\mu_i)| > \dfrac{\pi}{2n}$ for all eigenvalues μ_i. Turing instability occurs when this condition is violated for some wave number $k \neq 0$.

The eigenvalue from the first factor satisfies the following condition $|\arg(\mu_3)| = \pi > \frac{\pi}{2n}$ for any $n \geq 1$, so the dynamics is always stable when $K > 0$.

For Turing bifurcation analysis, we consider the critical case where the eigenvalues lie on the stability boundary. At the bifurcation point, let $\mu = \omega e^{i\theta}$ with $\theta = \dfrac{\pi}{2n}$, we get $\mu^{n\alpha_1} = \omega^{n\alpha_1} e^{in\alpha_1\theta} = \omega^{n\alpha_1} e^{i\frac{n\alpha_1\pi}{2n}} = \omega^{n\alpha_1} e^{i\frac{\alpha_1\pi}{2}}$, and $\mu^{n\alpha_2} = \omega^{n\alpha_2} e^{i\frac{\alpha_2\pi}{2}}$, and substituting these into Eq (2.13) and separating real and imaginary parts, we get

$$\omega^{n(\alpha_1+\alpha_2)} \cos\left(\tfrac{(\alpha_1+\alpha_2)\pi}{2}\right) - q\omega^{n\alpha_1} \cos\left(\tfrac{\alpha_1\pi}{2}\right) - p\omega^{n\alpha_2} \cos\left(\tfrac{\alpha_2\pi}{2}\right) + (pq - rs) = 0, \tag{2.15}$$

$$\omega^{n(\alpha_1+\alpha_2)} \sin\left(\tfrac{(\alpha_1+\alpha_2)\pi}{2}\right) - q\omega^{n\alpha_1} \sin\left(\tfrac{\alpha_1\pi}{2}\right) - p\omega^{n\alpha_2} \sin\left(\tfrac{\alpha_2\pi}{2}\right) = 0. \tag{2.16}$$

From Eq (2.16), we can express one parameter in terms of others. For instance, solving for p

$$p = \frac{\omega^{n(\alpha_1+\alpha_2)} \sin\left(\tfrac{(\alpha_1+\alpha_2)\pi}{2}\right) - q\omega^{n\alpha_1} \sin\left(\tfrac{\alpha_1\pi}{2}\right)}{\omega^{n\alpha_2} \sin\left(\tfrac{\alpha_2\pi}{2}\right)}.$$

Substituting into Eq (2.15) and simplifying, we obtain the bifurcation condition. After algebraic manipulation, we get the critical wave number

$$k_c^2 = \frac{1}{2D_B D_W}\left[a_{11}D_W\Phi_1 + a_{22}D_B\Phi_2 \pm \sqrt{(a_{11}D_W\Phi_1 + a_{22}D_B\Phi_2)^2 - 4D_B D_W(a_{11}a_{22}\Phi_3 - a_{12}a_{21})}\right], \tag{2.17}$$

where

$$\Phi_1(\alpha_1,\alpha_2) = \frac{\sin\left(\tfrac{(\alpha_1+\alpha_2)\pi}{2}\right)}{\sin\left(\tfrac{\alpha_2\pi}{2}\right)}, \qquad \Phi_2(\alpha_1,\alpha_2) = \frac{\sin\left(\tfrac{(\alpha_1+\alpha_2)\pi}{2}\right)}{\sin\left(\tfrac{\alpha_1\pi}{2}\right)},$$
$$\Phi_3(\alpha_1,\alpha_2) = \frac{\sin\left(\tfrac{(\alpha_1+\alpha_2)\pi}{2}\right)}{\sin\left(\tfrac{\alpha_1\pi}{2}\right)\sin\left(\tfrac{\alpha_2\pi}{2}\right)} \cos\left(\frac{(\alpha_1-\alpha_2)\pi}{2}\right).$$

We set $\Lambda = 0.8, M = 0.1, P = 1.2, N = 0.3, R = 0.4, \Gamma = 0.5, Q = 0.2, K = 0.15$, and analyze stability of the system without diffusion at $\alpha = [0.9, 0.9, 0.8]$, and $\alpha = [1.2, 1.2, 1.2]$, as shown in Figure 1.

Figure 1 presents the stability behavior of the system without diffusion with fractional derivative orders $\alpha = [0.9, 0.9, 0.8]$ and $\alpha = [1.2, 1.2, 1.2]$. Stability analysis results show that, under the selected parameters, the system exhibits conditional instability at E_0 and stability at E_1, which provides a theoretical basis for the Turing instability that may occur after the diffusion term is introduced.

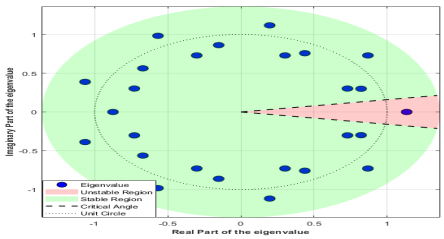

$E_0(0.0000, 4.0000, 1.3333)$ at $\alpha = [0.9, 0.9, 0.8]$

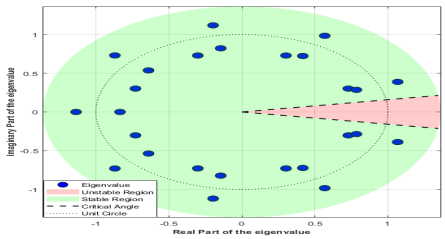

$E_1(0.9691, 4.0463, 1.3333)$ at $\alpha = [0.9, 0.9, 0.8]$

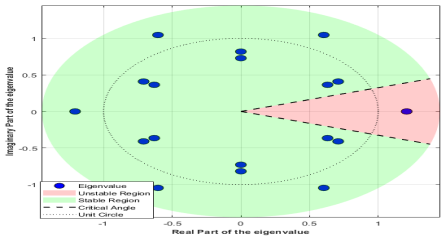

$E_0(0.0000, 4.0000, 1.3333)$ at $\alpha = [1.2, 1.2, 1.2]$

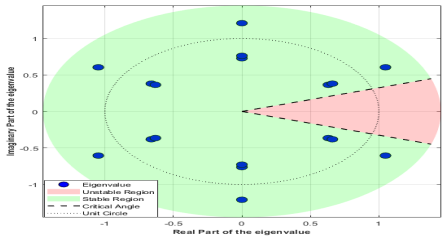

$E_1(0.9691, 4.0463, 1.3333)$ at $\alpha = [1.2, 1.2, 1.2]$

Figure 1. Stability of the system without diffusion at different fractional derivative orders.

Figure 2 illustrates the time-series evolution of the vegetation–water–salt system for different fractional derivative orders.

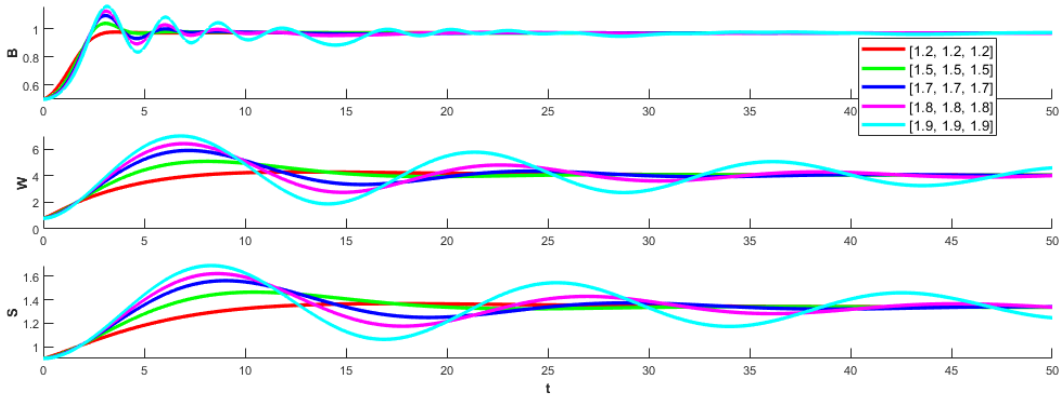

Figure 2. Comparison of time series plots at different fractional derivatives.

Figure 2 compares the dynamic behaviors under different fractional derivative orders. This comparison not only intuitively verifies the regulatory effect of the fractional order on the system dynamics, but also demonstrates its significant influence of the fractional order on the system behavior.

3. Numerical scheme

The numerical scheme is constructed around an accurate and stable discretization of the fractional time derivative. We commence with the Grünwald–Letnikov definition, which provides a natural foundation for numerical approximation.

Definition 3.1. *For a function $f(t)$, the α-th order Grünwald–Letnikov fractional derivative on the interval $[t_0, T]$ is defined as*

$$ {}_{t_0}\mathcal{D}_t^{\alpha} f(t) = \lim_{h\to 0} \frac{1}{h^{\alpha}} \sum_{j=0}^{\left\lfloor \frac{t-t_0}{h} \right\rfloor} (-1)^j \binom{\alpha}{j} f(t - jh), \tag{3.1} $$

where $\lfloor\cdot\rfloor$ denotes the floor function. The generalized binomial coefficients are expressed via the Gamma function

$$ \binom{\alpha}{j} = \frac{\Gamma(\alpha + 1)}{\Gamma(j + 1)\Gamma(\alpha - j + 1)}. \tag{3.2} $$

A straightforward numerical approximation at $t = t_k$ with a uniform time step τ is

$$ {}_{t_0}\mathcal{D}_{t_k}^{\alpha} f \approx \frac{1}{\tau^{\alpha}} \sum_{j=0}^{k} c_j f(t_{k-j}), \tag{3.3} $$

where $c_j = (-1)^j \binom{\alpha}{j}$. Direct evaluation of c_j using Gamma functions is numerically unstable for large j. A stable, recursive computation is therefore employed

$$ c_0 = 1, \qquad c_j = \left(1 - \frac{\alpha + 1}{j}\right) c_{j-1}, \quad j = 1, 2, \ldots, k. \tag{3.4} $$

The approximation (3.3) with coefficients from Eq (3.4) yields first-order accuracy, i.e., $O(\tau)$.

To achieve higher-order temporal accuracy, we replace the underlying first-order backward difference with a p-th order approximation, characterized by a polynomial generating function.

Definition 3.2. *A p-th order polynomial generating function for the first-order derivative is defined as*

$$ g_p(z) = \sum_{k=1}^{p} \frac{1}{k}(1 - z)^k = \sum_{k=0}^{p} \omega_k z^k. \tag{3.5} $$

The coefficients $\{\omega_k\}_{k=0}^{p}$ are uniquely determined by requiring that $g_p(z)$ approximates $-\ln(z)$ to p-th order accuracy near $z = 1$.

Theorem 3.3. *The coefficients $\{\omega_k\}_{k=0}^{p}$ in Eq* (3.5) *satisfy the following linear system of $p + 1$ equations:*

$$ \begin{cases} \sum_{k=0}^{p} \omega_k = 0, \\ \sum_{k=0}^{p} k\omega_k = -1, \\ \sum_{k=0}^{p} k^2\omega_k = -2, \\ \vdots \\ \sum_{k=0}^{p} k^p\omega_k = -p. \end{cases} \tag{3.6} $$

Proof. Starting from the identity $\sum_{k=0}^{p} \omega_k z^k = \sum_{k=1}^{p} \frac{1}{k}(1-z)^k$, we evaluate at $z = 1$ to obtain the first equation: $\sum_{k=0}^{p} \omega_k = 0$.

For the subsequent equations, we define the operator $\mathcal{L}_m[f] = \left(z\frac{d}{dz}\right)^m f(z)\Big|_{z=1}$. Applying $\mathcal{L}_m$ to both sides of the identity yields:

$$\mathcal{L}_m\left[\sum_{k=0}^{p} \omega_k z^k\right] = \sum_{k=0}^{p} k^m \omega_k.$$

Applying $\mathcal{L}_m$ to the right-hand side, $\sum_{k=1}^{p} \frac{1}{k}(1-z)^k$, and evaluating at $z = 1$ results in the constant $-m$ for $m = 1, 2, \ldots, p$. This is because the operator extracts the coefficient of the $(1-z)^m$ term, and the contributions from terms with $k > m$ vanish at $z = 1$. Equating both sides for each m produces the system Eq (3.6).

This framework is generalized to fractional derivatives.

Definition 3.4. *The p-th order generating function for the fractional derivative of order α is defined as*

$$g_p^{\alpha}(z) = \Big(g_p(z)\Big)^{\alpha} = \left(\sum_{k=0}^{p} \omega_k z^k\right)^{\alpha}. \tag{3.7}$$

Let its formal power series expansion be

$$g_p^{\alpha}(z) = \sum_{k=0}^{\infty} c_k^{(\alpha)} z^k. \tag{3.8}$$

Theorem 3.5. *The coefficients $c_k^{(\alpha)}$ in the expansion* (3.8) *can be computed via the following stable recurrence relation:*

$$\begin{aligned} c_0^{(\alpha)} &= \omega_0^{\alpha}, \\ c_m^{(\alpha)} &= \frac{1}{m\omega_0} \sum_{i=1}^{\min(m,p)} [i(1+\alpha) - m]\, \omega_i\, c_{m-i}^{(\alpha)}, \quad \text{for } m \geq 1, \end{aligned} \tag{3.9}$$

provided $\omega_0 \neq 0$.

Proof. From the definitions, we have $\left(\sum_{k=0}^{p} \omega_k z^k\right)^{\alpha} = \sum_{k=0}^{\infty} c_k^{(\alpha)} z^k$. Differentiating the identity

$$\left(\sum_{k=0}^{p} \omega_k z^k\right)\left(\sum_{k=0}^{\infty} c_k^{(\alpha)} z^k\right) = \left(\sum_{k=0}^{p} \omega_k z^k\right)^{1+\alpha}$$

with respect to z, multiplying by z, and equating coefficients of z^m yields, for $m \geq 1$,

$$\sum_{i=0}^{\min(m,p)} \omega_i (m-i) c_{m-i}^{(\alpha)} = (1+\alpha) \sum_{i=1}^{\min(m,p)} i\omega_i c_{m-i}^{(\alpha)}.$$

Isolating the term with $i = 0$ on the left (i.e., $\omega_0 m c_m^{(\alpha)}$) and rearranging gives

$$\omega_0 m c_m^{(\alpha)} = \sum_{i=1}^{\min(m,p)} [i(1+\alpha) - (m-i)]\, \omega_i c_{m-i}^{(\alpha)} = \sum_{i=1}^{\min(m,p)} [i(1+\alpha) - m]\, \omega_i c_{m-i}^{(\alpha)}.$$

Solving for $c_m^{(\alpha)}$ yields the recurrence relation (3.9).

The resulting high-order numerical approximation for the fractional time derivative at time level t_k is

$$ {}_{t_0}\mathcal{D}^{\alpha}_{t_k} f \approx \frac{1}{\tau^{\alpha}} \sum_{j=0}^{k} c_j^{(\alpha)} f(t_{k-j}), \tag{3.10} $$

which possesses a local truncation error of order $O(\tau^p)$.

For the spatial discretization of the reaction-diffusion system, we employ a nine-point finite difference stencil to approximate the two-dimensional Laplace operator ∇^2. This scheme provides improved accuracy and isotropy compared to the standard five-point formula.

The discrete Laplace operator at grid point (x_i, y_j) with uniform spacing h is given by

$$ \Delta_h \phi_{i,j} = \frac{1}{6h^2} \left[\phi_{i+1,j+1} + \phi_{i-1,j-1} + \phi_{i+1,j-1} + \phi_{i-1,j+1} + 4\left(\phi_{i+1,j} + \phi_{i-1,j} + \phi_{i,j+1} + \phi_{i,j-1}\right) - 20\phi_{i,j} \right], \tag{3.11} $$

where $\phi_{i,j}$ denotes the approximate solution at (x_i, y_j).

Applying the high-order fractional time discretization (3.10) together with the nine-point spatial discretization (3.11) to the vegetation–water–salinity model yields the following fully discrete system. Let $B^k_{i,j}$, $W^k_{i,j}$, and $S^k_{i,j}$ represent the discrete approximations for vegetation biomass, water, and salinity, respectively, at grid point (i, j) and time t_k. The scheme is

$$ \begin{cases} \frac{B^{k+1}_{i,j} - \sum_{m=0}^{N_k} c_m^{(\alpha_1)} B^{k-m}_{i,j}}{\tau^{\alpha_1}} = \Lambda W^k_{i,j} B^k_{i,j}(1 - B^k_{i,j}) - M B^k_{i,j} + D_B \Delta_h B^k_{i,j} \\ \frac{W^{k+1}_{i,j} - \sum_{m=0}^{N_k} c_m^{(\alpha_2)} W^{k-m}_{i,j}}{\tau^{\alpha_2}} = P - N(1 - R B^k_{i,j}) W^k_{i,j} - \Gamma \frac{(W^k_{i,j})^2}{(W^k_{i,j})^2 + 1} B^k_{i,j} + D_W \Delta_h W^k_{i,j} \\ \frac{S^{k+1}_{i,j} - \sum_{m=0}^{N_k} c_m^{(\alpha_3)} S^{k-m}_{i,j}}{\tau^{\alpha_3}} = Q - K S^k_{i,j} + D_S \Delta_h S^k_{i,j}, \end{cases} \tag{3.12} $$

where Δ_h is defined in Eq (3.11). Periodic boundary conditions are applied on the computational domain.

4. Numerical simulation of pattern dynamical behavior

Figures 3–7 illustrate the pattern formation and dynamical evolution of the vegetation-water-salinity system under different parameters and different fractional derivative combinations $(\alpha_1, \alpha_2, \alpha_3)$.

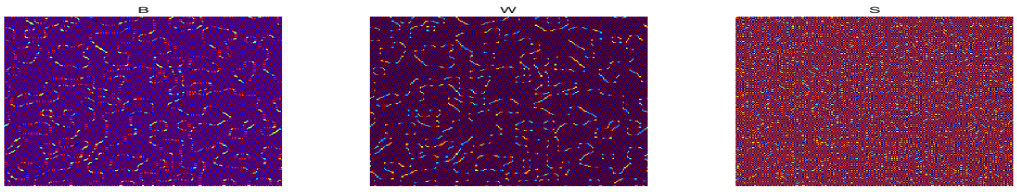

Figure 3. Numerical simulation results at $\alpha_1 = 0.9, \alpha_2 = 0.8, \alpha_3 = 1.0, \Lambda = 0.8, M = 0.1, P = 1.2, N = 0.5, R = 0.8, \Gamma = 0.5, Q = 0.2, K = 0.15, D_B = 1.5, D_W = 2.5, D_S = 5.0, h = 1.0, \tau = 0.1, n = 200$, and $m = 2000$.

Figure 3 presents the pattern evolution of the vegetation–water–salinity system under an asymmetric fractional–order setting, with $\alpha_1 = 0.9$, $\alpha_2 = 0.8$, $\alpha_3 = 1.0$, where plant biomass and soil water dynamics are modeled with sub-diffusive orders, while salt transport follows an integer-order description. The

simulation demonstrates the gradual emergence of irregular and fragmented vegetation patches over extended time scales, exhibiting weak connectivity and pronounced spatial heterogeneity.

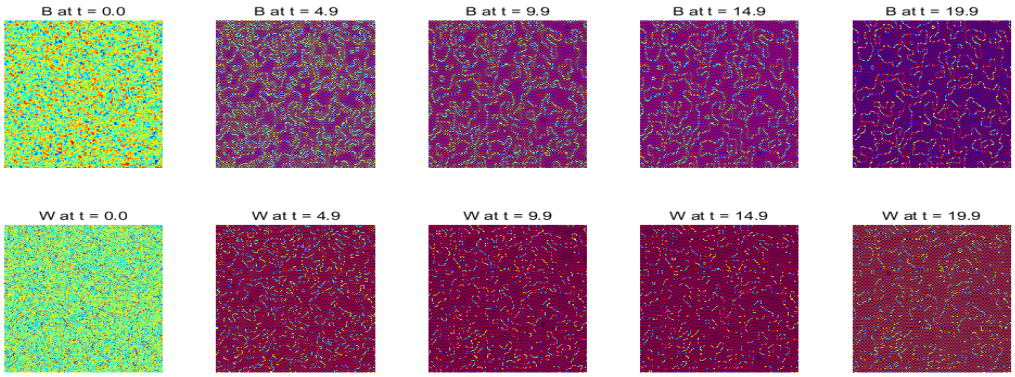

$\alpha_1 = 0.9, \alpha_2 = 0.8, \alpha_3 = 1.0$

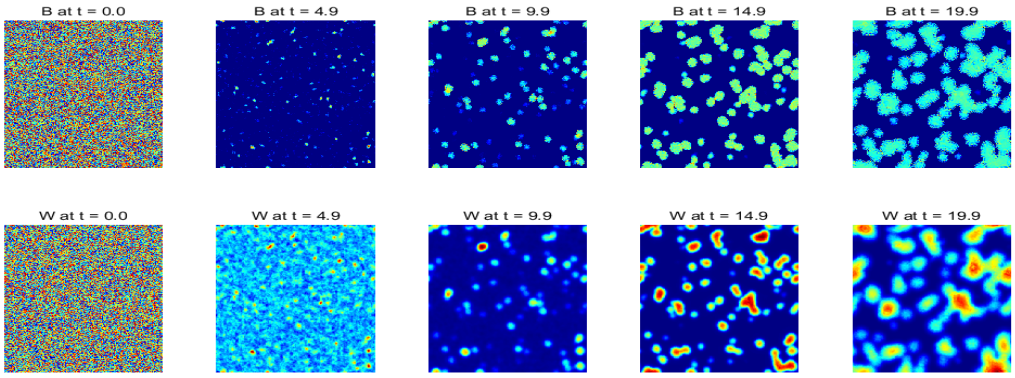

$\alpha_1 = 1.9, \alpha_2 = 1.8, \alpha_3 = 1.0$

Figure 4. Comparing the dynamic behavior of the patterns of different fractional derivatives at $\Lambda = 0.8, P = 1.2, N = 0.5, R = 0.8, \Gamma = 0.25, Q = 0.8, K = 0.5, D_B = 1.5, D_W = 2.5, D_S = 0.1, h = 1.0, \tau = 0.1, n = 200$, and $m = 300$.

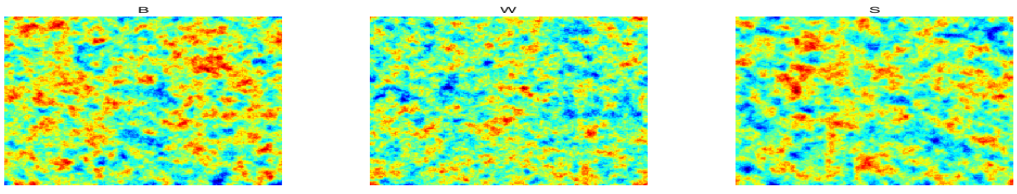

Figure 5. Numerical simulation results at $\alpha_1 = 1.2, \alpha_2 = 1.2, \alpha_3 = 1.2, \Lambda = 0.2, M = 0.01, P = 0.08, N = 0.03, R = 0.5, \Gamma = 0.6, Q = 0.05, K = 0.1, D_B = 1.0, D_W = 2.5, D_S = 2.0, h = 1.0, \tau = 0.1, n = 200$, and $m = 30,000$.

In Figure 4, a comparison of the dynamic behavior and pattern formation for different fractional derivative orders $(\alpha_1, \alpha_2, \alpha_3)$. This figure illustrates how the memory effects and non-local properties inherent in fractional calculus significantly influences the spatiotemporal evolution of the system.

displays the temporal evolution from homogeneous initial conditions to stationary patterns, demonstrating the developmental dynamics.

Figure 5 illustrates the pattern dynamics under fully super–diffusive orders $\alpha = [1.2, 1.2, 1.2]$. Compared to lower-order cases, vegetation patterns emerge more rapidly, forming a regular, compact, and uniformly distributed patches. The simulations show that patterns reach steady–state rapidly, with sharp edges, highlighting the role of super–diffusion in accelerating material transport and propagation. These results suggest that the fractional-order models with $\alpha > 1$ are particularly effective for capturing the dynamics of ecosystems with rapid response mechanisms, such as fast water infiltration or salt migration.

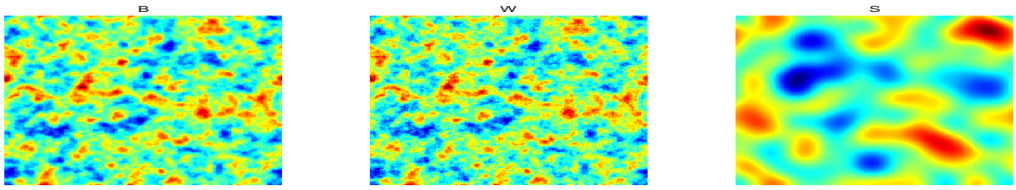

Figure 6. Numerical simulation results at $\alpha_1 = 1.0, \alpha_2 = 0.9, \alpha_3 = 1.0, \Lambda = 0.8, M = 0.1, P = 1.2, N = 0.3, R = 0.4, \Gamma = 0.5, Q = 0.2, K = 0.15, D_B = 1.0, D_W = 2.5, D_S = 2.0, h = 1.0, \tau = 0.1, n = 200$, and $m = 30,000$.

Figure 6 illustrates the pattern formation under the mixed-order setting $\alpha_1 = 1.0$, $\alpha_2 = 0.9$, and $\alpha_3 = 1.0$. The resulting vegetation patterns display transitional characteristics between classical Turing patterns and fractional-order patterns: patch structures are relatively regular but with slightly blurred edges, and their evolution exhibits noticeable memory-induced delays.

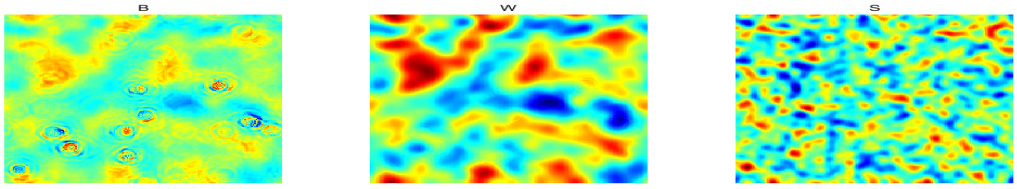

Figure 7. Numerical simulation results at $\alpha_1 = 1.9, \alpha_2 = 1.8, \alpha_3 = 1.0, \Lambda = 0.8, M = 0.1, P = 1.2, N = 0.5, R = 0.8, \Gamma = 0.5, Q = 0.2, K = 0.15, D_B = 1.0, D_W = 2.0, D_S = 0.1, h = 1.0, \tau = 0.1, n = 200$, and $m = 300$.

Figure 7 depicts the pattern formation and evolution of the vegetation–water–salinity system under a highly asymmetric fractional-order configuration with $\alpha_1 = 1.9$, $\alpha_2 = 1.8$, and $\alpha_3 = 1.0$. Simulation results show that the system forms highly regular vegetation patches with sharply defined boundaries in a very short time. The patches exhibit obvious grid-like or lattice-like arrangements, with significantly enhanced spatial periodicity.

5. Conclusions

In this paper, we systematically investigated the dynamics of a fractional-order vegetation–water–salinity model through both theoretical analysis and numerical simulations. The

bifurcation analysis highlights how fractional orders influence the Turing instability threshold and the resulting pattern selection mechanisms. The proposed high-order numerical scheme, which combines Grünwald–Letnikov discretization in time with a nine-point finite difference method in space, demonstrates superior accuracy and stability for the fractional reaction-diffusion systems. Our numerical results effectively capture a variety of vegetation patterns and their transitions under different ecological parameters, offering valuable insights into the complex interplay between memory effects, resource availability, and vegetation dynamics in arid ecosystems.

Use of AI tools declaration

The authors declare we have not used Artificial Intelligence (AI) tools in the creation of this article.

Acknowledgements

This paper is supported by the Jining Normal University Natural Science Key Research Project "In Intelligent Control of Wind Power Line Cruise under the Development Strategy of Green Electric Power+Super Computing Power" (Project No.: JSKY2024006), and as part of the phased achievements in the construction of the "University Physics" smart course and the autonomous region's top-tier course initiative. The Doctoral Innovation Research Fund Project of Jining Normal University: (jsbsjj2355), and Natural Science Foundation of Inner Mongolia (2025MS01012).

Conflict of interest

The authors declare that there are no conflicts of interest regarding the publication of this article.

Author contributions

Conceptualization, Methodology, Software, Data, Formal analysis and Funding acquisition, Writing-original draft and writing review and editing: Hai Yan Zhang, Wei Zhang, and Hao Lu Zhang. All authors have read and agreed to the published version of the manuscript.

References

1. J. A. Sherratt, A. D. Synodinos, Vegetation patterns and desertification waves in semi-arid environments: Mathematical models based on local facilitation in plants, *Discrete Contin. Dyn. Syst. Ser. B*, **17** (2012), 2815–2827. https://doi.org/10.3934/dcdsb.2012.17.2815
2. L. Eigentler, J. A. Sherratt, Effects of precipitation intermittency on vegetation patterns in semi-arid landscapes, *Phys. D*, **405** (2020), 132396. https://doi.org/10.1016/j.physd.2020.132396
3. M. H. Kabir, M. O. Gani, Numerical bifurcation analysis and pattern formation in a minimal reaction-diffusion model for vegetation, *J. Theor. Biol.*, **536** (2022), 110997. https://doi.org/10.1016/j.jtbi.2021.110997

4. I. Moreno-Villamil, D. A. Rueda-Gómez, É. J. Villamizar-Roa, On a cross-diffusion model in ecohydrology: Theory and numerics, *Acta Appl. Math.*, **196** (2025), 1. https://doi.org/10.1007/s10440-025-00708-y
5. M. Abbas, F. Giannino, A. Iuorio, Z. Ahmad, F. Calabrò, PDE models for vegetation biomass and autotoxicity, *Math. Comput. Simul.*, **228** (2025), 386–401. https://doi.org/10.1016/j.matcom.2024.07.004
6. A. Iuorio, N. Salvatori, G. Toraldo, F. Giannino, Analysis and numerical simulations of travelling waves due to plant-soil negative feedback, *Eur. J. Appl. Math.*, **35** (2024), 554–565. https://doi.org/10.1017/S0956792523000323
7. A. Iuorio, F. Veerman, The influence of autotoxicity on the dynamics of vegetation spots, *Phys. D*, **427** (2021), 133015. https://doi.org/10.1016/j.physd.2021.133015
8. X. L. Gao, H. L. Zhang, X. Y. Li, Research on pattern dynamics of a class of predator-prey model with interval biological coefficients for capture, *AIMS Math.*, **9** (2024), 18506–18527. https://doi.org/10.3934/math.2024901
9. H. L. Zhang, Y. L. Wang, J. X. Bi, S. H. Bao, Novel pattern dynamics in a vegetation-water reaction-diffusion model, *Math. Comput. Simul.*, **241** (2026), 97–116. https://doi.org/10.1016/j.matcom.2025.09.020
10. S. Zhang, H. L. Zhang, Y. L. Wang, Z. Y. Li, Dynamic properties and numerical simulations of a fractional phytoplankton-zooplankton ecological model, *Networks Heterog. Media*, **20** (2025), 648–669. https://doi.org/10.3934/nhm.2025028
11. J. Y. Yang, Y. L. Wang, Z. Y. Li, Exploring dynamics and pattern formation of a fractional-order three-variable Oregonator model, *Networks Heterog. Media*, **20** (2025), 1201–1229. https://doi.org/10.3934/nhm.2025052
12. L. Eigentler, J. A. Sherratt, Metastability as a coexistence mechanism in a model for dryland vegetation patterns, *Bull. Math. Biol.*, **81** (2019), 2290–2322. https://doi.org/10.1007/s11538-019-00606-z
13. C. Y. Gai, T. Kolokolnikov, Resource-mediated competition between two plant species with different rates of water intake, *SIAM J. Appl. Math.*, **83** (2023), 576–602. https://doi.org/10.1137/21M144623X
14. P. Broadbridge, B. H. Bradshaw-Hajek, D. Triadis, Exact non-classical symmetry solutions of Arrhenius reaction-diffusion, *Proc. R. Soc. A*, **471** (2015), 20150580. https://doi.org/10.1098/rspa.2015.0580
15. P. Broadbridge, B. H. Bradshaw-Hajek, A. J. Hutchinson, Conditionally integrable PDEs, non-classical symmetries and applications, *Proc. R. Soc. A*, **479** (2023), 20230209. https://doi.org/10.1098/rspa.2023.0209
16. P. Broadbridge, C. Rogers, On a nonlinear reaction-diffusion boundary-value problem: Application of a Lie-Backlund symmetry, *J. Aust. Math. Soc. Ser. B Appl. Math.*, **34** (1993), 318–332. https://doi.org/10.1017/S0334270000008924
17. Z. Y. Li, M. C. Wang, Y. L. Wang, Solving a class of variable order nonlinear fractional integral differential equations by using reproducing kernel function, *AIMS Math.*, **7** (2022), 12935–12951. https://doi.org/10.3934/math.2022716

18. Z. Y. Li, Y. L. Wang, F. G. Tan, X. H. Wan, H. Yu, J. S. Duan, Solving a class of linear nonlocal boundary value problems using the reproducing kernel, *Appl. Math. Comput.*, **265** (2015), 1098–1105. https://doi.org/10.1016/j.amc.2015.05.117
19. Y. L. Wang, L. N. Jia, H. L. Zhang, Numerical solution for a class of space-time fractional equation by the piecewise reproducing kernel method, *Int. J. Comput. Math.*, **96** (2019), 2100–2111. https://doi.org/10.1080/00207160.2018.1544367
20. X. Y. Li, Y. L. Wang, Z. Y. Li, Numerical simulation for the fractional-in-space Ginzburg–Landau equation using Fourier spectral method, *AIMS Math.*, **8** (2023), 2407–2418. https://doi.org/10.3934/math.2023124
21. C. Han, Y. L. Wang, Z. Y. Li, Numerical solutions of space fractional variable-coefficient KdV-modified KdV equation by Fourier spectral method, *Fractals*, **29** (2021), 2150246. https://doi.org/10.1142/S0218348X21502467
22. C. Han, Y. L. Wang, Z. Y. Li, Novel patterns in a class of fractional reaction-diffusion models with the Riesz fractional derivative, *Math. Comput. Simul.*, **202** (2022), 149–163. https://doi.org/10.1016/j.matcom.2022.05.037
23. H. L. Zhang, Z. Y. Li, X. Y. Li. Numerical simulation of pattern and chaos dynamic behaviour in the fractional-order-in-time Lengyel-Epstein reaction-diffusion system, *Int. J. Comput. Math.*, 1–21. https://doi.org/10.1080/00207160.2025.2612196
24. D. Y. Xue, *Fractional Calculus and Fractional-Order Control*, Beijing, Science Press, 2018.
25. D. Y. Xue, L. Bai, Numerical algorithms for Caputo fractional-order differential equations, *Int. J. Control*, **90** (2016), 1201–1211. https://doi.org/10.1080/00207179.2016.1158419
26. D. Y. Xue, C. N. Zhao, Y. Q. Chen, A modified approximation method of fractional order system, in *Proceedings of IEEE Conference on Mechatronics and Automation*, (2006), 1043–1048. Luoyang, China. https://doi.org/10.1109/ICMA.2006.257769
27. I. Petráš, *Fractional-order Nonlinear Systems: Modeling, Analysis and Simulation*, Springer Science & Business Media, 2011.

AIMS Press